Heliyon 9 (2023) e22514

Contents lists available at ScienceDirect

Heliyon

journal homepage: www.cell.com/heliyon

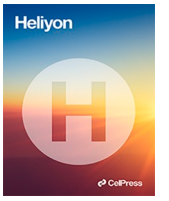

Fe_3O_4 microplate filled PEI matrix composite with remarkable nonlinear conductive characteristics, dielectric property, and low percolation threshold

Haoyuan Wang, Hengfeng Li *

School of Materials Science and Engineering, Central South University, Changsha, 410083, China

ARTICLE INFO

Keywords:
Field grading
Nonlinear conductivity
Dielectric property
Fe_3O_4 microplate
Polyetherimide

ABSTRACT

As the presence of a percolating network formed by filler is indispensable for field grading composite, particulate fillers often result in high filler content that can be unfavorable in some aspects. The utilization of fillers with high aspect ratio is an effective way of reducing percolation threshold. In this work, Fe_3O_4 microplate (FMP) was prepared by a PVP-assisted hydrothermal method and it was adopted to fabricate composite films with different filler content by using polyetherimide (PEI) as the matrix. The composite film exhibited a percolation threshold of approximately 8 phr. The nonlinear coefficient measured 6.28 at a filler content of 10 phr. The nonlinearity in the conductive behavior of the composites was attributed to tunneling effect and Schottky emission. The filling of the FMP into PEI resulted in increase in dielectric constant and the dielectric loss maintained low. This study suggests that the FMP is a promising filler of low-filler-content field grading composite.

1. Introduction

High-voltage transmission has been a more and more important method of dealing with the globally increasing demand of energy [1]. However, since high voltage is involved, its development is raising concerns about problems such as partial discharge, electric field distortion and even electrical failure, endangering the safety of electrical systems [2,3]. It is feasible to alleviate such problems by applying protective measures, including using field grading materials which possess nonlinear conductivity to realize nonlinear resistive field grading. These materials show insulating behavior at low electric fields, while under electric fields higher than a threshold value, their conductivities significantly enhance.

Basically, field grading material is a composite incorporating polymer matrix and conductive or semiconductive particles, such as ZnO, SiC, carbon black, etc. [4]. There must be a continuous and complete percolating network consisted of fillers in the polymer matrix for carriers to travel along at high electric fields to induce nonlinearity in conductive performance of the composite [5]. Therefore, utilizing particulate fillers typically necessitates a filler loading to reach the percolation threshold. It can cause disadvantages in terms of heavy weight, worse flexibility of the composite and overheating at high electric fields. These problems can be effective mitigated by adopting two-dimensional fillers as they have large aspect ratios which are conducive to achieve low percolation threshold. A few studies have paid attention to using several types of two-dimensional materials, such as graphene oxide [6,7], graphite nanoplatelet [8], tungsten disulfide [9] and MXene [10], as fillers of field grading composites. Dielectric properties of Fe_3O_4

* Corresponding author.
E-mail address: lihf@csu.edu.cn (H. Li).

https://doi.org/10.1016/j.heliyon.2023.e22514
Received 12 April 2023; Received in revised form 30 October 2023; Accepted 14 November 2023
Available online 19 November 2023
2405-8440/© 2023 The Authors. Published by Elsevier Ltd. This is an open access article under the CC BY-NC-ND license (http://creativecommons.org/licenses/by-nc-nd/4.0/).

particles and Fe_3O_4 filled composites with different polymer matrices, including poly(vinylidene fluoride), epoxy and polystyrene, were studied by other researchers [11–14]. Fe_3O_4 particle has also been mentioned as a traditional filler of field grading composites in a few literatures [1,5]. However, the use of two-dimensional Fe_3O_4 as filler of field grading composite has yet to be reported. Polyimide has been widely applied in composites for electrical insulation by virtue of its mechanical performance, insulation property and thermal stability [15]. There are many subgroups of polyimide and among them polyetherimide (PEI) shows enhanced processability [16]. In this study, Fe_3O_4 microplate (FMP) was synthesized and filled in polyetherimide (PEI) to prepare polymer matrix composite films with various filler loadings. I–V tests and dielectric measurements were carried out to study the potential of FMP functioning as the filler of field grading composite with low filler content.

2. Experimental

2.1. Materials

PEI granules (Ultem 1000, Sabic) was dried in vacuum under 60 °C overnight before being used as the polymer matrix for preparation of the composites. Potassium ferricyanide, sodium hydroxide (NaOH), polyvinylpyrrolidone (PVP, K30) and ammonia hydroxide were provided by Sinopharm Chemical Reagent Co., Ltd.

2.2. Preparation of Fe_3O_4 microplate

FMP was fabricated by a facile one-pot hydrothermal process. Half a gram of potassium ferricyanide, 1.5 g of NaOH, 8 g of PVP, 60 mL of deionized water and 5 mL of ammonia hydroxide were introduced into a 100 mL Teflon lining, which was then sealed in an autoclave and kept at 140 °C for 12 h for the synthesis. After that, deionized water and alcohol were used to wash the products through centrifugation.

2.3. Preparation of FMP filled PEI composite films

PEI was used as the polymer matrix of the composites. A specific quantity of FMP was dispersed in NMP (4 mL) via sonication. After that, 1 g of PEI granules was introduced in the mixture and it was mechanically stirred under 70 °C until the PEI fully dissolved, resulting in a precursor mixture. The composite film was prepared by applying the precursor mixture onto a glass substrate using the blade coating method. Then the glass substrate was positioned in a vacuum oven at 60 °C for 12 h to allow the majority of the NMP to evaporate. Residual solvent was removed by raising the temperature to 220 °C and keeping for another 4 h. A group of composite films with various filler loadings were fabricated. Thickness of each film was approximately 50 μm. A schematic of the process of preparation of FMP/PEI films is displayed in Fig. 1.

2.4. Characterizations

Morphology of FMP and cross-sections of the composite films were observed by scanning electron spectroscopy (SEM, TESCAN MIRA3 LMH, 20 kV) equipped with energy-dispersive X-ray spectroscopy (EDS, Ultim Max 20) and transmission electron spectroscopy (TEM, Tecnai G^2 20, accelerating voltage: 200 kV). Samples were treated by sputtering to coat gold before the SEM characterizations. A few amounts of the FMP were dispersed in ethanol to form a mixture and then the mixture was dropped on a copper TEM grid for the TEM characterization. Structure and composition of FMP was studied by X-ray diffraction (XRD, D/max 2550 VB, 40 kV, 250 mA, step size: 0.02°, scan speed: 8°/min 2 theta range: 10–80°), X-ray photoelectron spectroscopy (XPS, Thermo K-Alpha+, 15 kV, 10 mA, spot size: 400 μm) and Fourier transform infrared spectroscopy (FTIR, Nicolet 6700, sample preparation: KBr pellet method, wavenumber range: 400-4000 cm^{-1}). Dielectric properties of the composite films were measured by a Keysight E4990A impedance analyzer (test voltage: 1 V). DC *I* (current)-*V* (voltage) characteristics of the composite films were studied using a Keithley 2470 sourcemeter at a voltage ramp rate of 50 V/(mm·s). A gold electrode having 4 mm diameter was coated on each side of the composite film sample through sputtering by an ion sputtering instrument (SBC 12, KYKY, China) before the dielectric and *I–V* measurements which were conducted at room temperature. Results of *I–V* tests were expressed by converting the data to electric field (*E*), current density (*J*) and conductivity (σ) according to the equations below, where *S* and *d* represent the area of the electrode and the thickness of the film, respectively:

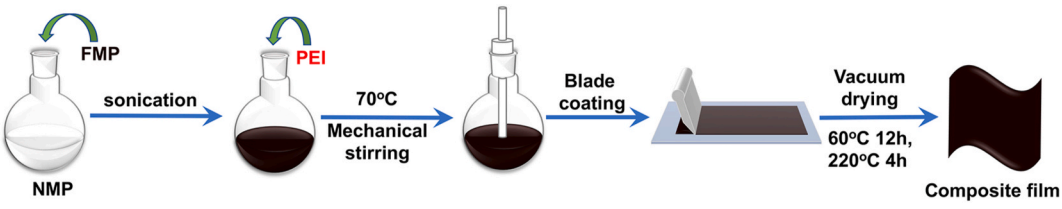

Fig. 1. Procedures of preparation of the composite films.

$$J = I/S \tag{1}$$

$$E = V/d \tag{2}$$

$$\sigma = J/E \tag{3}$$

3. Results and discussion

3.1. Characterizations of FMP and the composite films

The SEM image of FMP is demonstrated in Fig. 2a. It demonstrates that two-dimensional FMPs with a small number of particles were produced during the hydrothermal reaction. The FMP is generally large with lateral size from a few to tens of microns. Fig. 2b is the TEM image of some FMPs. The overlapping of the microplates indicates that they are relatively thin. The high-resolution TEM image (Fig. 2c) suggests that the FMP is well crystallized with a lattice spacing of 2.57 Å, which is correlative to the {311} facet of Fe_3O_4 [17,18]. The selected area electron diffraction (SAED) pattern displayed in Fig. 2d conforms to the crystal structure of face-centered cubic Fe_3O_4 and suggests the single-crystalline structure of the FMP [19].

XPS survey spectrum of FMP is shown in Fig. 3a. It indicates that the FMP contain iron, oxygen, carbon, and a small amount of nitrogen. The two peaks at 711 eV and 724.9 eV in the XPS curve of Fe 2p (Fig. 3b) are corresponding to Fe $2p_{3/2}$ and Fe $2p_{1/2}$ of Fe_3O_4, respectively [20,21]. In the XPS spectrum of N 1s (Fig. 3c), a peak at 399.5 eV which is correlative to the C–N group of the pyrrolidone unit of PVP is observed [22], suggesting that a small amount of PVP molecules were adhered to the surface of the FMP. The peak at 258.8 eV in the C 1s spectrum (Fig. 3d) ascribes to the C–N group [23,24], further proving the adsorption of PVP on the surface of FMP. Except for the adventitious carbon contamination from the atmosphere, the peaks at 284.7 eV and 287.7 eV in the C 1s spectrum are also corresponding to the C–C and C═C group of PVP. The peak at 529.6 eV in the O 1s spectrum (Fig. 3e) is corresponding to the lattice oxygen of Fe–O of FMP [25]. The peak at 530.9 eV ascribes to the hydroxyl groups at the chain ends of PVP as the production process of commercially available PVP makes them terminated in hydroxyl groups [26–28]. The peak at 532 eV associates with the C═O group of the pyrrolidone unit of PVP [23,29].

FTIR spectra of FMP and PVP (K30) are displayed in Fig. 4a. The broad absorption band at 3431 cm^{-1} of the spectrum of PVP corresponds to O–H stretching vibration. The absorption bands at 2956 cm^{-1} and 1659 cm^{-1} are corelative to C–H asymmetric

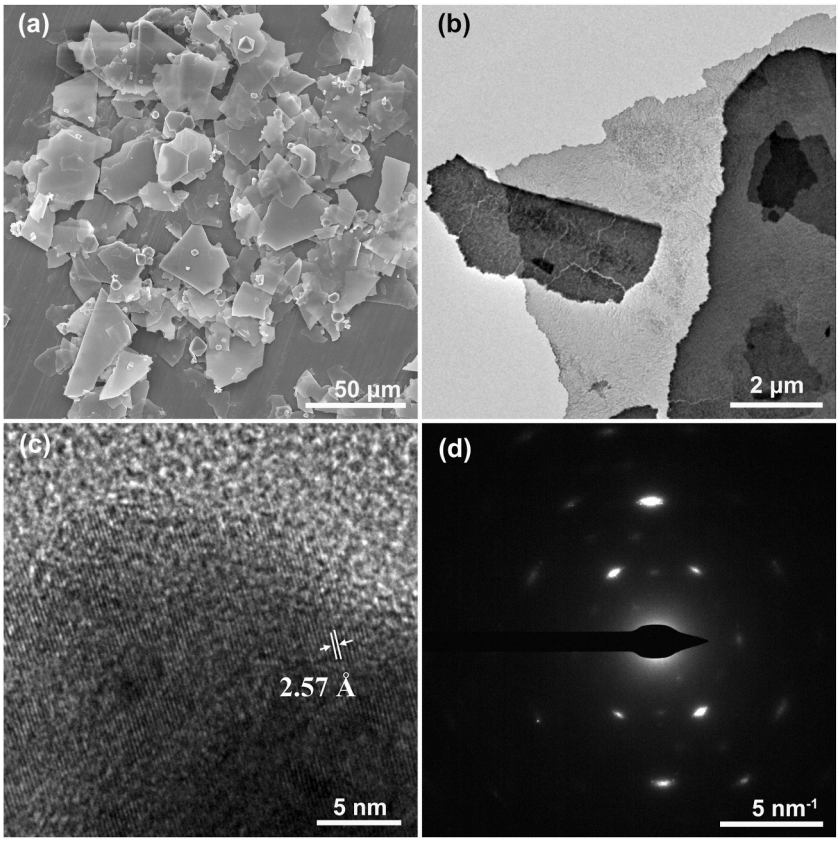

Fig. 2. SEM image (a), TEM image (b), High-resolution TEM image (c) and SAED patten of FMP.

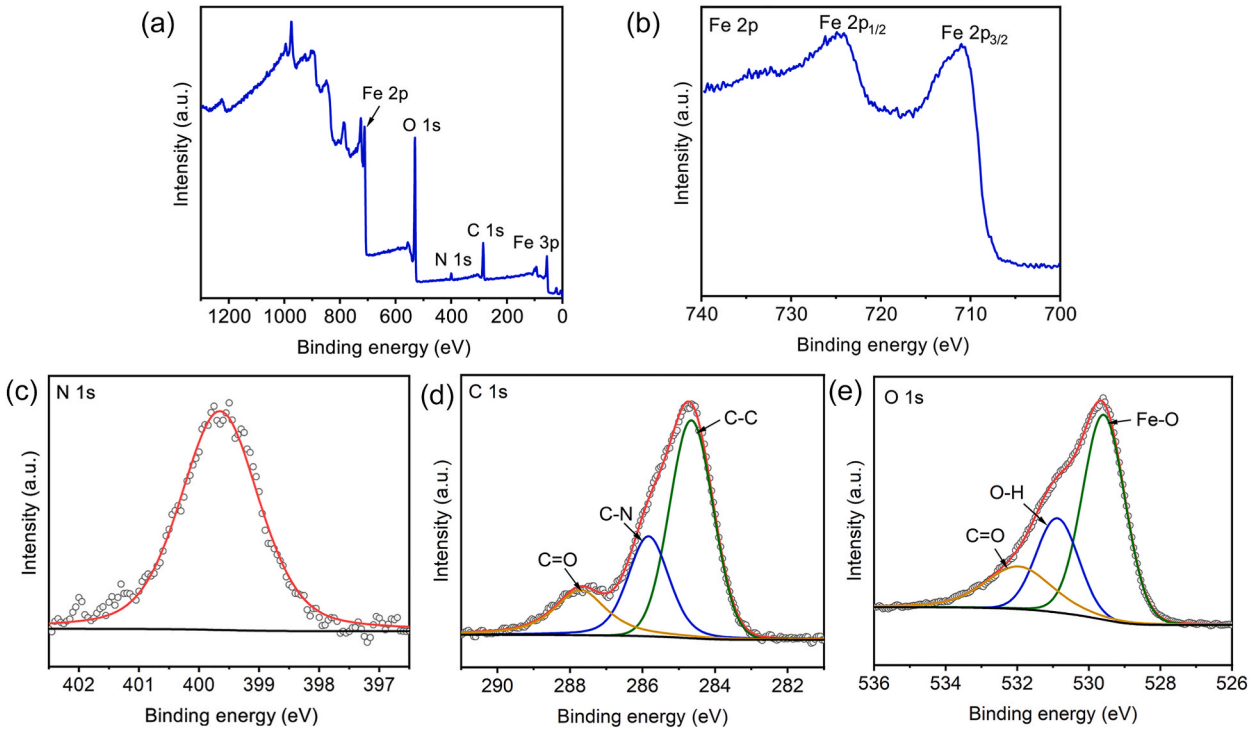

Fig. 3. (a) XPS survey spectrum of FMP; XPS spectra of (b) Fe 2p, (c) N1s, (d) C 1s and (e) O 1s of FMP.

stretching vibration and C═O stretching vibration, respectively [30]. The absorption bands at 1464 cm^{-1} and 1427 cm^{-1} are characteristic bands of pyrrolidinyl group, while the absorption bands at 1290 cm^{-1} and 1020 cm^{-1} are corresponding to C–N vibrations [31,32]. The absorption bands of O–H, C–H and C═O vibrations of PVP are also shown on the FTIR spectrum of FMP, further proving the adsorption of PVP. XRD pattern of FMP shown in Fig. 4b conforms to the standard XRD pattern of Fe_3O_4 (JCPDS No.89-4319, magnetite, syn). XRD patterns of PEI matrix composite films with different filler loadings are demonstrated in Fig. 4c. The amorphous nature of PEI is indicated by the broad peak centered at around 19°. XRD characteristics peaks of FMP also appear on the XRD pattern of the composites, indicating that FMP is stable in the PEI matrix and no reactions are happened between FMP and PEI during fabrication procedures of the composite films.

SEM images of the cross sections of the composite films are presented in Fig. 5a–d. Distribution of FMP in PEI is reflected by the EDS elemental mapping of Fe (Fig. 5e–h). The cross sections are produced by fracturing the composite samples in liquid nitrogen. It shows from the cross sections that there is almost no holes or filler protrusions observed at the filler-matrix interfaces, indicating that FMP is firmly combined with the PEI matrix. Oxygen and nitrogen atoms locate in the backbone of PEI chain. Therefore, there are hydrogen bonding effect between the PEI matrix and the commercially available PVP which is adsorbed on FMP. Compatibility between the filler and the matrix is then enhanced to realize strong interfacial interaction at the filler-matrix interface and uniform distribution of the fillers in the matrix. In addition, the hydrophobic carbon chains of PVP are also contributed to the uniform distribution of the fillers in PEI as they provide repulsive force to avoid agglomeration of the fillers [33]. It shows that the FMPs are only tens to hundreds of nanometers thick, leading to large aspect ratio.

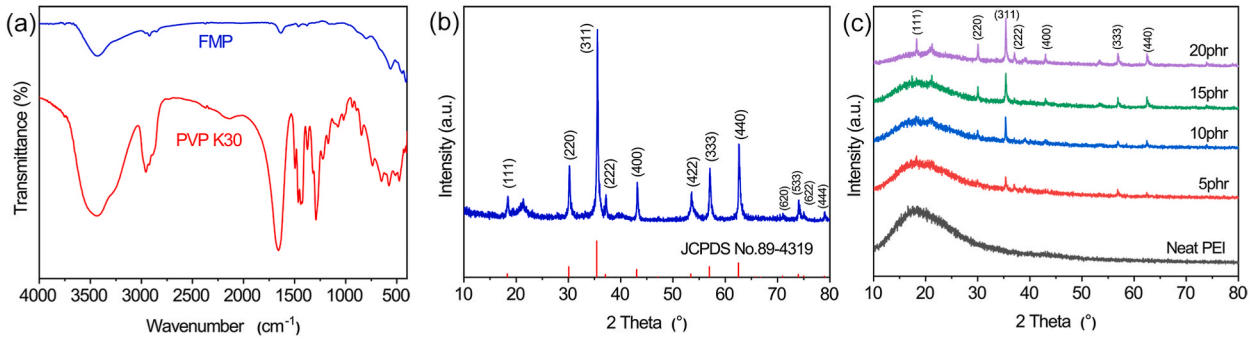

Fig. 4. (a) FTIR spectrum of the FMP and PVP (K30); (b) XRD pattern of FMP; (c) XRD pattern of the composite films with different filler loadings.

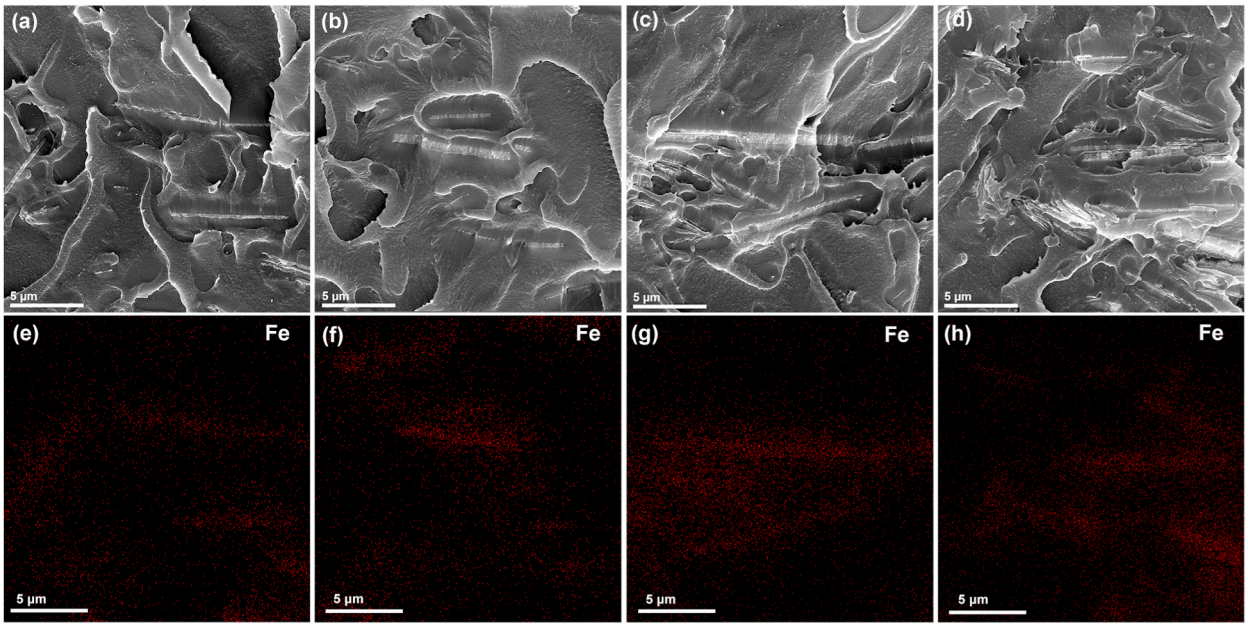

Fig. 5. SEM images and EDS elemental mapping of cross sections of (a, e) 5phr, (b, f) 10 phr, (c, g) 15 phr and (d, h) 20 phr of the FMP filled PEI composite films.

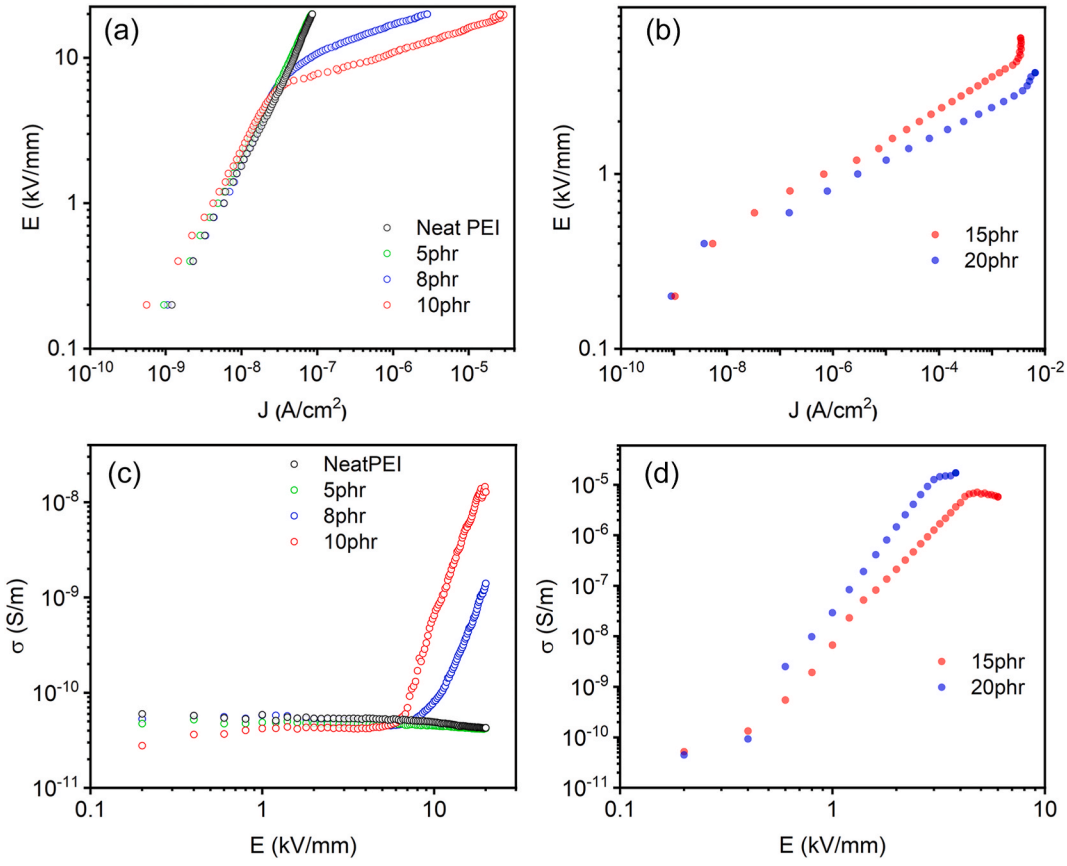

Fig. 6. *E-J* (a–b) and *σ-E* (c–d) relationships of FMP/PEI composite films.

3.2. DC nonlinear conductivity of the composite films

Nonlinearity in the field-dependent conductive performance of FMP filled PEI matrix composite films are shown in Fig. 6. Almost ohmic conductive characteristics were observed for neat PEI and the 5 phr of the FMP filled composite as their conductivities are low and stable under the growing electric field, while nonlinear conductive performances are shown by the composites with filler content of not less than 8 phr. It indicates that the percolating network was not formed within the polymer matrix when it contains 5 phr of the filler. Motion of carriers was then hindered by the thick polymer layer residing between short path made of the fillers even at strong electric fields, and therefore, nonlinear conductivity was not performed. The results in Fig. 6 suggest that the percolation threshold of FMP/PEI is around 8 phr, which is relatively low. It can be ascribed to the large aspect ratio of FMPs and the uniform distribution of the fillers in the PEI matrix.

Switching field is defined as the electric field above which conductivity of the field grading material begins to significantly elevate to show nonlinear conductive performance. Switching fields of the 8 phr and 10 phr of the FMP filled composite films are around 10.6 kV/mm and 7.0 kV/mm, respectively, as presented in Fig. 6c. While for the 15 phr and 20 phr of FMP filled composite films, the switching field is as low as about 0.6 kV/mm. Conductivity saturation describes the behavior that rising rate of conductivity of the composite slows down when the electric field elevates to a specific level [6]. The σ-E relationships of the composites filled by 10 phr, 15 phr and 20 phr of FMP demonstrate conductivity saturation behaviors at high electric fields as shown in Fig. 6c and d. It is caused by joule heating effect which is getting influential at high electric fields and leading to thermal expansion of the composite, resulting in degradation of the filler network [34]. Hence, regular E-J or σ-E relationship of a nonlinear conductive composite comprises three regions including the pre-switch region, the nonlinear region, and the conductivity saturation region, and they are divided by switching field and conductivity saturation point.

Tunneling effect and Schottky emission are two of the most adopted dielectric theories of explaining nonlinear conductivity of field grading materials. In tunneling effect theory, the nonlinear J-E characteristic is expressed by Fowler-Nordheim's equation [35]:

$$J = AE^2 \exp(B/E) \tag{4}$$

where A and B are constants. According to the equation, $\ln(J/E^2)$ is linear with $1/E$. Relationships of $\ln(J/E^2)$ against $1/E$ before the conductivity saturation of the 8–20 phr of FMP filled composites are presented in Fig. 7a and b. The relationship between $\ln(J/E^2)$ and

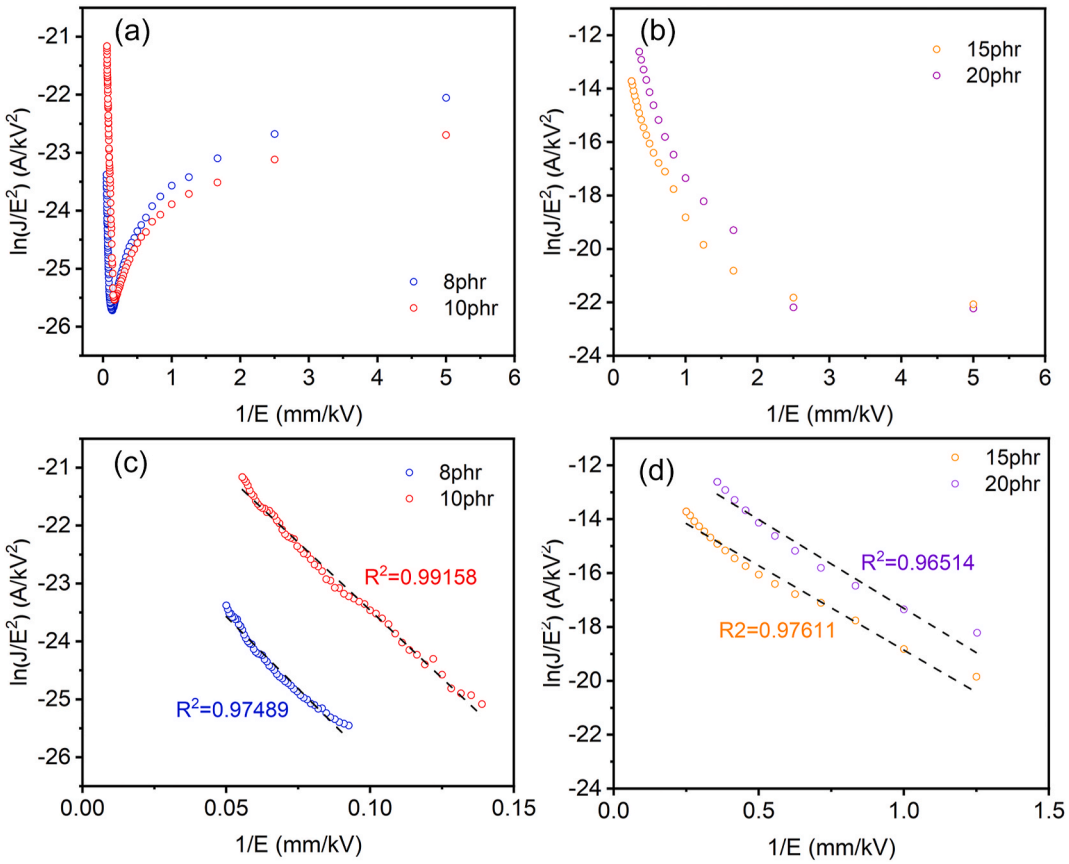

Fig. 7. Tunneling effect investigation of the FMP/PEI films: (a–b) before the conductivity saturation regions; (c–d) the nonlinear regions.

$1/E$ is almost linear at high electric fields. Linear fit is conducted for the $\ln(J/E^2)$-$1/E$ relationships within the nonlinear region as demonstrated in Fig. 7c and d. The R^2 values are all larger than 0.96, suggesting high goodness of linear fit and indicating that the nonlinear *E-J* relationships conform to tunneling effect. In Schottky emission theory, the nonlinear *J-E* relationship complies with this equation [35]:

$$J = A^* T^2 \exp\left(\beta E^{1/2} - q\Phi\right) \tag{5}$$

where T is the absolute temperature, A^* is a constant, Φ is the Schottky barrier height, q is the electric charge and β is a constant. According to this equation, $\ln J$ is linear with $E^{1/2}$. It shows in Fig. 8 that the $\ln J$-$E^{1/2}$ relationships of the composite films are also almost linear at high electric fields, especially in the nonlinear region as the R^2 values are all larger than 0.97, suggesting high goodness of linear fit and indicating that the *E-J* relationships follow Schottky emission theory. Hence, nonlinear conductivity of the FMP filled PEI matrix composite films was driven by the collaboration of tunneling effect and Schottky emission.

Function of barriers are involved in tunneling effect and Schottky emission [4]. In the FMP/PEI composite, barriers are mainly at the filler contacts. Due to differences in Fermi level and work function, Schottky-like barrier can form between an FMP and the PVP adsorbed on the surface of it [5]. Hence, back-to-back double Schottky barrier forms at the filler contact (Fig. 9). Under low electric fields, carrier motion is impeded by the barrier. While under high electric fields, the barrier height tilts and carriers have higher energy, causing more carriers passing through the barrier by tunneling effect and Schottky emission to induce electric field enhanced nonlinear conductive behavior.

A larger number and straighter conduction paths tend to build at a higher filler loading. Therefore, a lower filler content usually results in longer and more winding conduction path consisted of a larger number of fillers with more filler contacts, leading to more barriers in the conduction path [3,36,37]. Switching field is strongly affected by the number of barriers involved in the conduction path as each barrier has a characteristic voltage and carriers are able to traverse the barrier when subjected to voltage stronger than it [6]. Therefore, a low filler loading usually results in a higher switching field of the composite. Generally, there are more filler path in the filler network built by a higher loading of fillers. Hence, a higher filler loading usually results in a stronger conductivity of the composite at high electric fields (as shown in Fig. 6c and d) as there are more effective conduction paths being activated. The conductivities of the 8 phr and 10 phr of FMP filled composites are poor and close to that of neat PEI under weak electric fields. It is important since field grading materials should be highly resistive under weak electric fields. However, conductivities of the composites

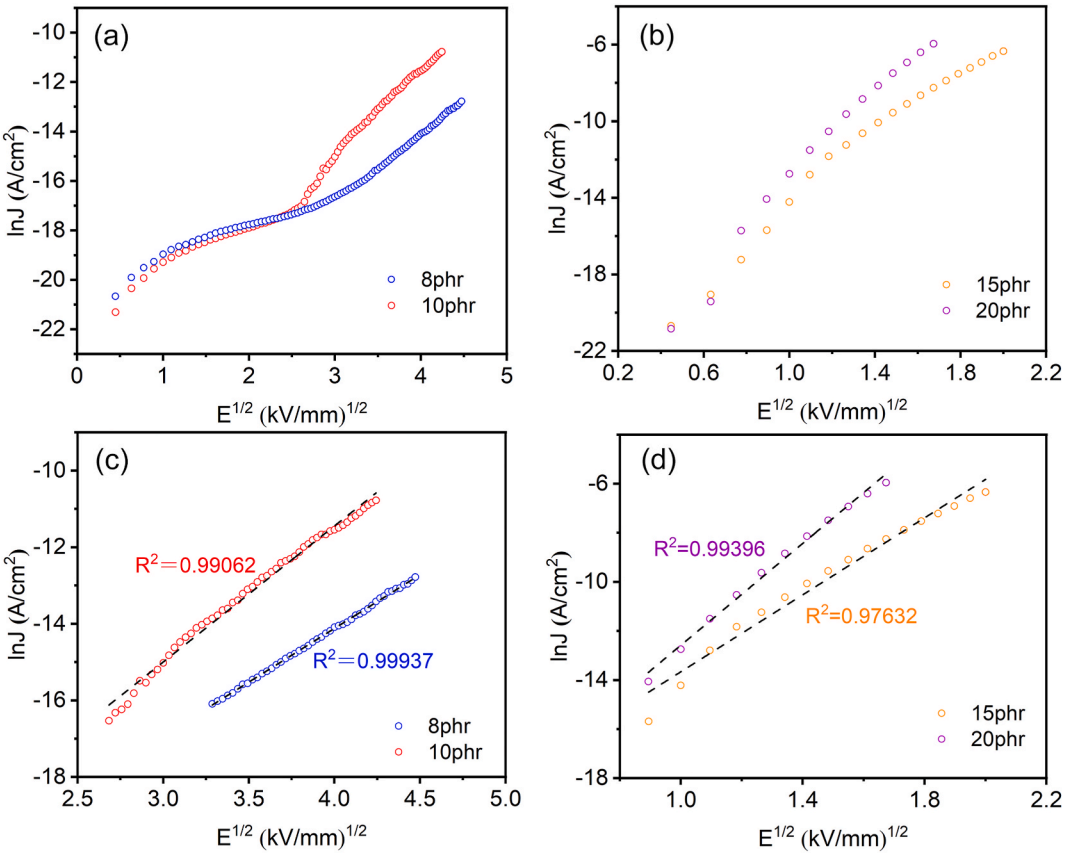

Fig. 8. Schottky emission analysis of the FMP/PEI composite films: (a–b) before the conductivity saturation regions; (c–d) the nonlinear regions.

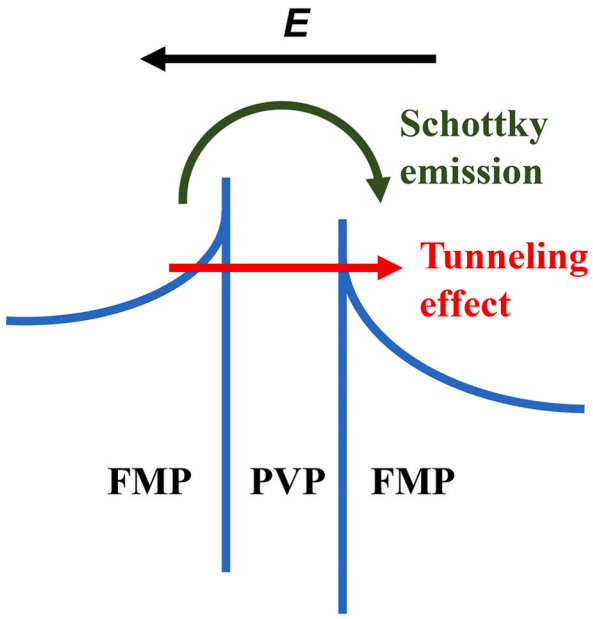

Fig. 9. Schematic of tunneling effect and Schottky emission at filler contact under applied electric field.

with filler content of 15 phr and 20 phr are much larger than that of neat PEI even under weak electric fields (0.6 kv/mm). At high filler content, there are abundant conduction paths in the composite. Therefore, the switching field becomes low, and conductivity begins to rapidly increase at low electric field. Although the composites filled by 15 phr and 20 phr of FMP showed remarkable nonlinear conductive performance, they are probably not proper candidates for field grading applications as their insulating features under low electric fields are compromised.

Nonlinear coefficient measures the field grading ability of the material under electric field between the switching field and the conductivity saturation point. It is obtained by the equation below [38]:

$$\alpha = \frac{d \ln J}{d \ln E} \tag{6}$$

Nonlinear coefficients of the composites filled by 8 phr and 10 phr of the FMP are 5.37 and 6.28, respectively. Conductivity of composite containing 10 phr of the FMP enhanced for approximately 3 magnitudes within 20 kV/mm. The nonlinear conductive characteristics of the composite fabricated in this work and a few other composites mentioned in literatures adopting traditional fillers such as SiC and ZnO, or other two-dimensional fillers are shown in Table 1. The FMP/PEI composite demonstrated competitive property with regard to the overall performance of nonlinear conductivity and low percolation threshold.

3.3. Dielectric properties of FMP/PEI composites

Materials exhibiting nonlinear conductive behavior with elevated dielectric constants are also beneficial for capacitive field grading, which is regarded as another main class of field grading method, in addition to resistive field grading [45]. Dielectric properties of the FMP filled PEI films are demonstrated in Fig. 10. Dielectric constants of the composites reduced with rise of frequency as the interfacial polarization at the filler-matrix interface was not able to keep up with frequency of the applied electric field [46], and therefore, loss caused by dielectric relaxation was getting more significant, generally leading to higher dielectric loss. Dielectric constant of PEI was increased with the addition of FMP filler. For instance, dielectric constant of PEI containing 8 phr of FMP was 5.8 at 1 kHz. The rise of dielectric constant was caused by interfacial polarization, microcapacitor effect and hydrogen bonding effect [47, 48]. Interfacial polarization of a composite is caused by free charges accumulating at the interface between filler and matrix. The FMPs show large aspect ratio and specific surface area. Thus, there is substantial interfacial area between FMP and PEI matrix in the composite films to induce significant interfacial polarization which promotes the rise of dielectric constant. The two-dimensional FMP can also cause prominent microcapacitor effect in the composites. It shows in Fig. 5a–d that there are some FMPs almost horizontally distribute in the PEI matrix during the film preparation process. These FMPs can act as the parallel electrodes of a microcapacitor and the PEI matrix between them plays the role of the dielectric layer. Then, there are such microcapacitors in the composites to strengthen the dielectric constant of the composite. Hydrogen bonds formed between the PEI matrix and the PVP adsorbed on the FMP result in formations of dipoles which also enhance the dielectric constants of the composites.

It shows in Fig. 10 that the dielectric losses of the FMP filled PEI composites are still kept on low level. Dielectric loss is generally caused by dielectric relaxation and leakage current [6]. For composites adopting fillers having high aspect ratios, such as the FMP/PEI composite, leakage current has a significant contribution to the source of dielectric loss in light of their low percolation thresholds.

Table 1
Comparative analysis of nonlinear conductive characteristics of field grading composites.

Composite (filler/matrix)	Filler content	Nonlinear coefficient	Percolation threshold	Ref.
FMP/PEI	10 phr	6.28	~8 phr	This work
Reduced graphene oxide/PDMS	3 phr	16	2~3 phr	[6]
Graphite nanoplatelet/Silicone rubber	5 wt%	3	4 wt%	[8]
WS_2/EPDM	40 phr	4.27	–	[9]
$Ti_3C_2T_x$/PEI	6 phr	10.18	2 phr	[10]
ZnO powder/EPDM	30 phr	1.83	20~30 phr	[39]
Micro-ZnO/PDMS	30 vol%	6.51	20~30 vol%	[40]
ZnO whisker/Silicone rubber	5 vol%	4.53	2.4 vol%	[41]
ZnO microvaristor/Silicone rubber	39 vol%	12.5	39 vol%	[37]
SiC whisker/PDMS	30 phr	1.19	–	[42]
β-SiC powder/PDMS	15 vol%	2.81	–	[43]
α-SiC particle/PDMS	50 wt%	1.04	–	[44]

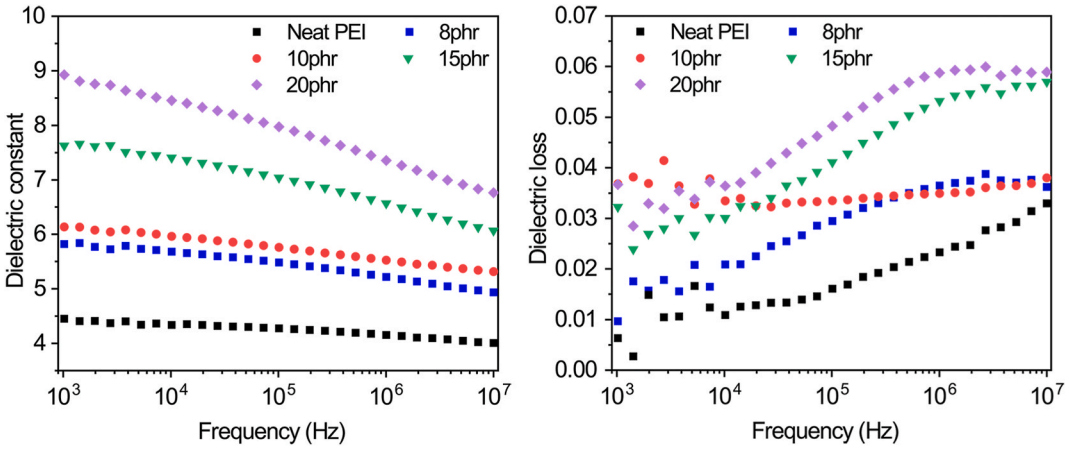

Fig. 10. Dielectric properties of the FMP filled PEI composite films.

Leakage current in the FMP/PEI composite under low electric fields was inhibited by the barriers of the FMP network, leading to low dielectric loss. It is in line with with the *I–V* measurements shown in Fig. 6 as the FMP/PEI composites are as insulating as neat PEI at very weak electric fields.

4. Conclusions

Fe_3O_4 microplates (FMP) with surface adsorption of PVP was successfully synthesized. Nonlinear conductive behavior and dielectric properties of the FMP filled PEI were studied. Percolation threshold of the composite was as low as around 8 phr. The composite presented a nonlinear coefficient of 6.28 with a filler loading of 10 phr. Nonlinearity in the conductive behavior of the composite complies with tunneling effect and Schottky emission. Dielectric constant of the composite was enhanced with the introduction of the FMP filler, while the dielectric loss was remaining low. The work of this paper demonstrated that FMP has great potential of acting as the filler of field grading composite with low filler content. The aspect ratio of FMP and property study of the composites were limited. Further study can focus on making Fe_3O_4 nanosheet with higher aspect ratio and study other electrical performance, such as dielectric breakdown, of the composites.

Data availability

Data will be made available on request.

CRediT authorship contribution statement

Haoyuan Wang: Writing – review & editing, Writing – original draft, Methodology, Investigation, Formal analysis, Data curation, Conceptualization. **Hengfeng Li:** Writing – review & editing, Supervision, Project administration, Methodology, Investigation, Funding acquisition, Conceptualization.

Declaration of competing interest

The authors declare that they have no known competing financial interests or personal relationships that could have appeared to influence the work reported in this paper.

Acknowledgment

This work is supported by the National Natural Science Foundation of China (51573209).

References

[1] A. Can-Ortiz, L. Laudebat, Z. Valdez-Nava, S. Diaham, Nonlinear electrical conduction in polymer composites for field grading in high-voltage applications: a review, Polymers 13 (9) (2021) 1370, https://doi.org/10.3390/polym13091370.
[2] X.L. Zhao, X. Yang, J. Hu, Q. Li, J.L. He, Globally reinforced mechanical, electrical, and thermal properties of nonlinear conductivity composites by surface treatment of varistor microspheres, Compos. Sci. Technol. 175 (2019) 151–157, https://doi.org/10.1016/j.compscitech.2019.03.018.
[3] X.L. Zhao, X. Yang, Q. Li, J.L. He, J. Hu, Synergistic effect of ZnO microspherical varistors and carbon fibers on nonlinear conductivity and mechanical properties of the silicone rubber-based material, Compos. Sci. Technol. 150 (2017) 187–193, https://doi.org/10.1016/j.compscitech.2017.07.025.
[4] P. Han, J.W. Zha, S.J. Wang, Z.M. Dang, Theoretical analysis and application of polymer-matrix field grading materials in HVDC cable terminals, High Volt. 2 (1) (2017) 39–46, https://doi.org/10.1049/hve.2016.0067.
[5] L. Donzel, F. Greuter, T. Christen, Nonlinear resistive electric field grading Part 2: materials and applications, IEEE Electr. Insul. Mag. 27 (2) (2011) 18–29, https://doi.org/10.1109/Mei.2011.5739419.
[6] Z.P. Wang, J.K. Nelson, H. Hillborg, S. Zhao, L.S. Schadler, Graphene oxide filled nanocomposite with novel electrical and dielectric properties, Adv. Mater. 24 (23) (2012) 3134–3137, https://doi.org/10.1002/adma.201200827.
[7] M. Wahlander, F. Nilsson, R.L. Andersson, A. Carlmark, H. Hillborg, E. Malmstrom, Reduced and surface-modified graphene oxide with nonlinear resistivity, Macromol. Rapid Commun. 38 (16) (2017), 1700291, https://doi.org/10.1002/marc.201700291.
[8] R. Metz, C. Blanc, S. Dominguez, S. Tahir, R. Leparc, M. Hassanzadeh, Nonlinear field dependent conductivity dielectrics made of graphite nanoplatelets filled composites, Mater. Lett. 292 (2021), 129611, https://doi.org/10.1016/j.matlet.2021.129611.
[9] P. Han, J.W. Zha, M.S. Zheng, Y.Q. Wen, Z.M. Dang, Nonlinear electric conductivity and thermal conductivity of WS_2/EPDM field grading materials, J. Appl. Phys. 122 (19) (2017), 195106, https://doi.org/10.1063/1.4996261.
[10] H.Y. Wang, H.F. Li, MXene filled polyetherimide matrix composites with remarkable nonlinear conductive performance and low percolation threshold, Compos. Sci. Technol. 216 (2021), 109062, https://doi.org/10.1016/j.compscitech.2021.109062.
[11] K. Iwauchi, Dielectric properties of fine particles of Fe_3O_4 and some ferrites, Jpn. J. Appl. Phys. 10 (11) (1971), 1520, https://doi.org/10.1143/JJAP.10.1520.
[12] H.Y. Wang, Q. Fu, J.Q. Luo, D.M. Zhao, L.H. Luo, W.P. Li, Three-phase Fe_3O_4/MWNT/PVDF nanocomposites with high dielectric constant for embedded capacitor, Appl. Phys. Lett. 110 (24) (2017), 242902, https://doi.org/10.1063/1.4986443.
[13] L.A. Ramajo, A.A. Cristóbal, P.M. Botta, J.M.P. López, M.M. Reboredo, M.S. Castro, Dielectric and magnetic response of Fe_3O_4/epoxy composites, Compos. Part A-Appl. S. 40 (4) (2009) 388–393, https://doi.org/10.1016/j.compositesa.2008.12.017.
[14] P.N. Vakil, F. Muhammed, D. Hardy, T.J. Dickens, S. Ramakrishnan, G.F. Strouse, Dielectric properties for nanocomposites comparing commercial and synthetic Ni- and Fe_3O_4-loaded polystyrene, ACS Omega 3 (10) (2018) 12813–12823, https://doi.org/10.1021/acsomega.8b01477.
[15] V.E. Ogbonna, A.P.I. Popoola, O.M. Popoola, S.O. Adeosun, A review on polyimide reinforced nanocomposites for mechanical, thermal, and electrical insulation application: challenges and recommendations for future improvement, Polym. Bull. 79 (1) (2022) 663–695, https://doi.org/10.1007/s00289-020-03487-8.
[16] Z. Xu, Z.L. Croft, D. Guo, K. Cao, G.L. Liu, Recent development of polyimides: synthesis, processing, and application in gas separation, J. Polym. Sci. 59 (11) (2021) 943–962, https://doi.org/10.1002/pol.20210001.
[17] J.H. Zhang, Q.H. Kong, J. Du, D.K. Ma, G.C. Xi, Y.T. Qian, Formation, characterization, and magnetic properties of Fe_3O_4 micro octahedrons, J. Cryst. Growth 308 (1) (2007) 159–165, https://doi.org/10.1016/j.jcrysgro.2007.06.011.
[18] X.M. Liu, J.K. Kim, Solvothermal synthesis and magnetic properties of magnetite nanoplatelets, Mater. Lett. 63 (3–4) (2009) 428–430, https://doi.org/10.1016/j.matlet.2008.11.001.
[19] F.X. Ma, X.Y. Sun, K. He, J.T. Jiang, L. Zhen, C.Y. Xu, Hydrothermal synthesis, magnetic and electromagnetic properties of hexagonal Fe_3O_4 microplates, J. Magn. Magn Mater. 361 (2014) 161–165, https://doi.org/10.1016/j.jmmm.2014.02.092.
[20] H. Chen, H.J. Luo, Y.C. Lan, T.T. Dong, B.J. Hu, Y.P. Wang, Removal of tetracycline from aqueous solutions using polyvinylpyrrolidone (PVP-K30) modified nanoscale zero valent iron, J. Hazard Mater. 192 (1) (2011) 44–53, https://doi.org/10.1016/j.jhazmat.2011.04.089.
[21] Y.J. Meng, Y.D. Wang, L.J. Liu, Y.G. Fang, F.Q. Ma, C.H. Zhang, H.X. Dong, Efficient and magnetically recoverable U (VI) adsorbent: Fe_3O_4 loaded hypercrosslink copoly (styrene/maleic anhydride), Colloid. Surface. 632 (2022), 127644, https://doi.org/10.1016/j.colsurfa.2021.127644.
[22] F.X. Qiao, Y. Zhao, W.N. Zhang, J.H. Yang, Isoliquiritigenin nanosuspension enhances cytostatic effects in A549 lung cancer cells, Planta Med. 86 (8) (2020) 538–547, https://doi.org/10.1055/a-1134-3378.
[23] D.L. He, Y. Wang, L.Y. Zhang, S.L. Song, Y. Deng, Poly(vinylidene fluoride)-Based composites modulated via multiscale two-dimensional fillers for high dielectric performances, Compos. Sci. Technol. 159 (2018) 162–170, https://doi.org/10.1016/j.compscitech.2018.02.040.
[24] S.B. Tu, Q. Jiang, X.X. Zhang, H.N. Alshareef, Large dielectric constant enhancement in MXene percolative polymer composites, ACS Nano 12 (4) (2018) 3369–3377, https://doi.org/10.1021/acsnano.7b08895.
[25] A. Sionkowska, M. Wisniewski, H. Kaczmarek, J. Skopinska, P. Chevallier, D. Mantovani, S. Lazare, V. Tokarev, The influence of UV irradiation on surface composition. of collagen/PVP blended films, Appl. Surf. Sci. 253 (4) (2006) 1970–1977, https://doi.org/10.1016/j.apsusc.2006.03.048.
[26] H. Sun, P. Yu, X. Peng, L.Z. Meng, M. Qin, X.Y. Xu, J.S. Li, Inspired by the periodontium: a Universal bacteria-defensive Hydrogel for preventing percutaneous device-related infection, ACS Appl. Mater. Interfaces 14 (44) (2022) 50424–50433, https://doi.org/10.1021/acsami.2c15478.
[27] J. Xu, H.B. Yang, W.Y. Fu, Y.M. Sui, H.Y. Zhu, M.H. Li, G.T. Zou, Preparation and characterization of carbon fibers coated by Fe_3O_4 nanoparticles, Mat. Sci. Eng. B-Solid 132 (3) (2006) 307–310, https://doi.org/10.1016/j.mseb.2006.04.038.
[28] Y.J. Xiong, I. Washio, J.Y. Chen, H.G. Cai, Z.Y. Li, Y.N. Xia, Poly(vinyl pyrrolidone): a dual functional reductant and stabilizer for the facile synthesis of noble metal nanoplates in aqueous solutions, Langmuir 22 (20) (2006) 8563–8570, https://doi.org/10.1021/la061323x.
[29] T. Yamashita, P. Hayes, Analysis of XPS spectra of Fe^{2+} and Fe^{3+} ions in oxide materials, Appl. Surf. Sci. 254 (8) (2008) 2441–2449, https://doi.org/10.1016/j.apsusc.2007.09.063.
[30] S. Sethia, E. Squillante, Solid dispersion of carbamazepine in PVPK30 by conventional solvent evaporation and supercritical methods, Int. J. Pharm. (Amst.) 272 (1–2) (2004) 1–10, https://doi.org/10.1016/j.ijpharm.2003.11.025.
[31] H. Liu, B. Zhang, H.Q. Shi, Y.J. Tang, K. Jiao, X. Fu, Hydrothermal synthesis of monodisperse Ag(2)Se nanoparticles in the presence of PVP and KI and their application as oligonucleotide labels, J. Mater. Chem. 18 (22) (2008) 2573–2580, https://doi.org/10.1039/b719207j.
[32] S. Selvam, M. Sundrarajan, Functionalization of cotton fabric with PVP/ZnO nanoparticles for improved reactive dyeability and antibacterial activity, Carbohydr. Polym. 87 (2) (2012) 1419–1424, https://doi.org/10.1016/j.carbpol.2011.09.025.
[33] R. Si, Y.W. Zhang, L.P. You, C.H. Yan, Self-organized monolayer of nanosized ceria colloids stabilized by poly(vinylpyrrolidone), J. Phys. Chem. B 110 (12) (2006) 5994–6000, https://doi.org/10.1021/jp057501x.

[34] C.C. Lin, W.S. Lee, C.C. Sun, W.H. Whu, A varistor-polymer composite with nonlinear electrical-thermal switching properties, Ceram. Int. 34 (1) (2008) 131–136, https://doi.org/10.1016/j.ceramint.2006.09.018.
[35] X.T. Zhao, J. Guo, K. Wang, T.H. De Beauvoir, B. Li, C.A. Randall, Introducing a ZnO-PTFE (polymer) nanocomposite varistor via the cold sintering process, Adv. Eng. Mater. 20 (7) (2018), 1700902, https://doi.org/10.1002/adem.201700902.
[36] X. Yang, J. Hu, S.M. Chen, J.L. He, Understanding the percolation characteristics of nonlinear composite dielectrics, Sci. Rep. 6 (2016), 30597, https://doi.org/10.1038/srep30597.
[37] L. Gao, X. Yang, J. Hu, J.L. He, ZnO microvaristors doped polymer composites with electrical field dependent nonlinear conductive and dielectric characteristics, Mater. Lett. 171 (2016) 1–4, https://doi.org/10.1016/j.matlet.2016.02.016.
[38] T. Christen, L. Donzel, F. Greuter, Nonlinear resistive electric field grading Part 1: theory and simulation, IEEE Electr. Insul. Mag. 26 (6) (2010) 47–59, https://doi.org/10.1109/Mei.2010.5599979.
[39] Q.G. Chi, Y.Y. Hao, T.D. Zhang, C.H. Zhang, Q.G. Chen, X. Wang, Study on nonlinear conductivity and breakdown characteristics of zinc oxide-hexagonal boron nitride/EPDM composites, J. Mater. Sci. Mater. Electron. 29 (23) (2018) 19678–19688, https://doi.org/10.1007/s10854-018-0093-y.
[40] X.T. Zhang, M.Q. Le, V.C. Nguyen, J.F. Mogniotte, J.F. Capsal, D. Grinberg, P.J. Cottinet, L. Petit, Characterization of micro-ZnO/PDMS composite structured via dielectrophoresis-Toward medical application, Mater. Des. 208 (2021), 109912, https://doi.org/10.1016/j.matdes.2021.109912.
[41] J.K. Nie, D. Hou, G.K. Wang, F. Guo, X. Chen, Preparation and nonlinear conductivity characteristics of silicone rubber filled with silver-coated tetrapod-shaped ZnO whiskers, J. Electron. Mater. 48 (4) (2019) 2517–2522, https://doi.org/10.1007/s11664-019-07026-8.
[42] Z.L. Li, B.X. Du, Z.R. Yang, J. Li, Effects of crystal morphology on space charge transportation and dissipation of SiC/silicone rubber composites, IEEE Trans. Dielectr. Electr. Insul. 24 (4) (2017) 2616–2625, https://doi.org/10.1109/Tdei.2017.006388.
[43] Z.H. Yang, P.H. Hu, S.J. Wang, J.W. Zha, Z.C. Guo, Z.M. Dang, Effect of nano-fillers distribution on the nonlinear conductivity and space charge behavior in SiC/PDMS composites, IEEE Trans. Dielectr. Electr. Insul. 24 (3) (2017) 1735–1742, https://doi.org/10.1109/Tdei.2017.006214.
[44] B.X. Du, Z.L. Li, Z.R. Yang, Field-dependent conductivity and space charge behavior of silicone rubber/SiC composites, IEEE Trans. Dielectr. Electr. Insul. 23 (5) (2016) 3108–3116, https://doi.org/10.1109/Tdei.2016.7736876.
[45] W.K. Pan, Y. Wang, H. Ding, E.Z. Shen, Z.S. Zhang, X. Yang, Z.Z. Wang, S. Akram, Nonlinear materials applied in HVDC gas insulated equipment: from fundamentals to applications, IEEE Trans. Dielectr. Electr. Insul. 28 (5) (2021) 1588–1603, https://doi.org/10.1109/Tdei.2021.009631.
[46] X.W. Cao, W.J. Zhao, X.J. Gong, D.L. Zhang, Q.J. Su, J.W. Zha, X.M. Yin, W. Wu, R.K.Y. Li, Mussel-inspired polydopamine functionalized silicon carbide whisker for PVDF composites with enhanced dielectric performance, Compos. Part A-Appl. S. 148 (2021), 106486, https://doi.org/10.1016/j.compositesa.2021.106486.
[47] S. Majumder, M. Sardar, B. Satpati, S. Kumar, S. Banerjee, Magnetization enhancement of Fe_3O_4 by attaching onto graphene oxide: an interfacial effect, J. Phys. Chem. C 122 (37) (2018) 21356–21365, https://doi.org/10.1021/acs.jpcc.8b04861.
[48] Y. Zhang, J.Y. Liu, S. Ma, Y.J. Zhang, X. Zhao, X.D. Zhang, Z.D. Zhang, Synthesis of PVP-coated ultra-small Fe_3O_4 nanoparticles as a MRI contrast agent, J. Mater. Sci. Mater. Med. 21 (4) (2010) 1205–1210, https://doi.org/10.1007/s10856-009-3881-3.